Inverse method applied to autonomous broadband hydroacoustic survey detects higher densities of zooplankton in near-surface aggregations than vessel-based net survey

Muriel Dunn[1,2*], Geir Pedersen[3], Sünnje L. Basedow[4], Malin Daase[4], Stig Falk-Petersen[1], Loïc Bachelot[5], Lionel Camus[1], and Maxime Geoffroy[2,4]

[1]Akvaplan-niva AS, Fram Centre, Postbox 6606, Stakkevollan, 9296 Tromsø, Norway

[2] Center for Fisheries Ecosystems Research, Fisheries and Marine Institute of Memorial University of Newfoundland and Labrador, St. John's, A1C 5R3, NL, Canada

[3] Institute for Marine Research, 5005 Bergen, Norway

[4] Department of Arctic and Marine Biology, UiT The Arctic University of Norway, 9019 Tromsø, Norway

[5] IFREMER, Laboratoire d'Océanographie Physique et Spatiale, 29280 Plouzané, France

*Corresponding author (email: mbd@akvaplan.niva.no)

Abstract

Throughout all oceans, aggregations of zooplankton and ichthyoplankton appear as horizontal sound scattering layers (SSLs) when detected with active acoustic techniques. Quantifying the composition and density of these layers is prone to sampling biases. We conducted a net and trawl survey of the epipelagic fauna in northern Norway (70˚N) in June 2018 while an autonomous surface vehicle equipped with a broadband echosounder (283-383 kHz) surveyed the same region. Densities from the autonomous hydroacoustic survey were calculated using forward estimates from the relative density from the net and trawl, and inversion estimates with statistical data-fitting. All four methods (net, trawl, acoustic forward and inverse methods) identified that copepods dominated the epipelagic SSL, while pteropods, amphipods and fish larvae were present in low densities. The density estimates calculated with the inverse method were higher for mobile zooplankton, such as euphausiid larvae, than with the other methods. We concluded that the inverse method applied to broadband autonomous acoustic surveys can improve density estimates of epipelagic

organisms by diminishing avoidance biases and increasing the spatio-temporal resolution of ship-based surveys.

Keywords: broadband acoustics, inversion, machine learning, autonomous surface vehicle, zooplankton

Introduction

Pelagic zooplankton and ichthyoplankton form dense horizontal aggregations throughout all oceans and represent an easily accessible food source for higher trophic levels. In the North Atlantic, these organisms funnel energy from primary producers to top predators such as marine mammals, seabirds, and the pelagic early life stages of larger fishes targeted by commercial fisheries, e.g., Atlantic cod (*Gadus morhua*) (Falk-Petersen and Hopkins, 1981; Solvang et al. 2021). Accurate density estimates of zooplankton and ichthyoplankton are thus needed to calculate and model energy transfer in marine environments.

The density of zooplankton and ichthyoplankton can be calculated for large volumes of water using hydroacoustic surveys because the aggregations appear as sound scattering layers (SSLs) when detected with echosounders (Dietz, 1948; Barham, 1966; Proud et al., 2018). At high latitudes, for example in the Fram Strait, the backscatter from the SSLs is usually much stronger in the epipelagic zone (< 200 m) than in the mesopelagic zone (> 200 m), suggesting that there is a higher density of biomass near the surface than below 200 m (Knutsen et al., 2017; Gjøsæter et al., 2020). Epipelagic SSLs of zooplankton, mainly euphausiids, copepods, amphipods, pteropods, and juvenile fish, have been detected with acoustics over high latitude shelves (Knutsen et al., 2017, Bandara et al., 2022), in fjords in Northern Norway (Falk-Petersen and Hopkins, 1981; Falk-Petersen and Kristiansen, 1985), and in deeper basins of the Barents Sea (Gjøsæter et al., 2020). However, density estimates of epipelagic organisms generally contain several biases because of 1) the draft of research vessels and the near-field of acoustic instruments which form a blind zone in the top ca. 10 m (e.g., Pedersen et al., 2019); 2) variation in detection probability with density and range (Appenzeller and Leggett, 1992; Demer and Hewitt, 1995; Simmonds and MacLennan, 2008); and 3) the sound and light emitted by research vessels (Trevorrow et al., 2005; De Robertis et al., 2012; Peña, 2019; Berge et al., 2020).

New technology can contribute to minimizing uncertainties in the detection and density estimates of epipelagic organisms. The recent development of autonomous surface and subsurface vehicles with compact and energy-efficient active acoustic systems reduces the blind zone as well as artificial noise and light sources compared to traditional acoustic surveys conducted from research vessels. These autonomous platforms also have the potential to increase the temporal and spatial scale of acoustic surveys (e.g., Mordy et al., 2017; De Robertis et al., 2019; Verfuss et al., 2019). Concomitantly, the development of broadband echosounders (Andersen et al., 2021) and scattering models for several taxonomic groups (Jech et al., 2015) have improved our ability to detect and characterise small (<1 cm) acoustic targets at a high vertical resolution.

Two methods can be used to estimate density from the acoustic signal scattered from dense epipelagic aggregations of zooplankton and ichthyoplankton in SSLs: the forward method and the inverse method. The forward method uses the relative density of each taxonomic group based on net and trawl samples from the survey region to allocate a proportion of the backscatter, the sound intensity reflected by the targets, for a density estimate of each taxonomic group (Love, 1975; Simmonds and MacLennan, 2008). However, each net or trawl is inherently selective (Skjoldal et al., 2013) depending on mesh size, net/trawl opening, tow speed, and species density (Pearcy et al., 1983; Battaglia et al., 2006; Moriarty et al., 2018). Ultimately, with the forward method, biases from net and trawl selectivity are transferred to the species density estimates. The inverse method rather directly calculates the density of each taxonomic group from acoustic data by optimising the densities based on the received backscatter and the scattering models of each species (Holliday, 1977). When applying the inverse method to broadband acoustics, the spectrum of the acoustic signal can be fully exploited to optimize the model fitting and calculations of density for each taxonomic group. Applying the inverse method to broadband acoustic data has the potential to reduce the bias from net and trawl selectivity and could increase the value of datasets from autonomous or remotely operated platforms with sparse net validation.

This study assessed zooplankton and ichthyoplankton density estimates in a near-surface SSL using four different methods: mesozooplankton net (MultiNet), macrozooplankton trawl (Tucker trawl), and the forward and inverse methods applied to broadband acoustic data collected with an autonomous surface vehicle. The survey was conducted as a case study in the Tromsøflaket area, a bank north of the northern Norwegian Sea (70˚ N). We deployed nets and trawls from a research vessel while an autonomous surface vehicle equipped with a broadband echosounder surveyed the same region (Camus et al., 2019). We also tested the applicability of using theoretical scattering models (Chu and Ye, 1999; Khodabandeloo et al., 2021) to reduce the dependence on relative density estimates from net and trawl sampling when conducting autonomous hydroacoustic surveys. The limitations of each method are discussed and we provide recommendations on combining sampling methods to increase the accuracy of zooplankton and ichthyoplankton studies.

Materials and methods

I. Study area and survey design

Tromsøflaket is comprised of a plateau (150 – 250 m depth) located at the southwestern entrance of the Barents Sea (Figure 1). The plateau is an area of high biological activity; some bank areas are heavily trawled as they support a rich community of commercially harvested fish (Olsen et al., 2010). It is a difficult region for traditional ecosystem sampling activity despite the relatively shallow bank because of the strong and variable currents (Bellec et al., 2008; Kędra et al., 2017).

Tromsøflaket was surveyed from June 20th to 29th, 2018, from the R/V *Helmer Hanssen* and an autonomous surface vehicle (Sailbuoy, Offshore Sensing, Bergen, Norway, www.sailbuoy.no). During the R/V *Helmer Hanssen* cruise, environmental data and biological samples were collected at 11 stations to estimate zooplankton and fish composition, density, and vertical distribution (Stations 7 to 17; Table 1). The Sailbuoy was deployed from the vessel at Station 7 on June 21st. It was picked up from Station 11 on June 22nd to fix issues with the storage of acoustic data and relaunched on June 24th at Station 9. The Sailbuoy left the study area on June 29th and was recovered south of Lofoten on August 22nd. The ship left the study area on June 25th. For this study, we only used the data from the Tromsøflaket region as delimited in Figure 1.

II. Biological sampling

Mesozooplankton were sampled by vertical hauls (towing speed 0.5 m s^{-1}) using a multiple opening/closing net (MultiNet, Hydro-Bios, Kiel, Germany, www.hydrobios.de; mouth opening 0.25 m^2, mesh size 180 μm). Five depth strata (bottom-100, 100-30, 30-10, 10-5, and 5-0 m) were sampled at each station, but data below 100 m were not used in this study because it was outside the range of the echosounder mounted on the Sailbuoy. At station 13, samples were taken by a ring net (WP2 net, Hydro-Bios), with the same mouth opening, mesh size and depth strata as the MultiNet, but did not include the 0-5 m depth stratum. All samples were preserved in 4% formaldehyde-in-seawater solution buffered with hexamine. Taxonomic analyses were completed in the laboratory. Large organisms (total length > 5 mm) were picked out using forceps, identified, and counted from the whole sample. The remainder of the sample was examined by sub-sampling with aliquots obtained with a 5 ml automatic pipette, with the pipette tip cut at 5 mm diameter to allow a free collection of mesozooplankton. The number of subsamples analysed was chosen so that at least 150 individuals of copepods (*Calanus* spp.) and 300 other organisms were counted. To assess the length frequency distribution of the *Calanus* population, the prosome length of all counted individuals of *Calanus* spp. was measured from the tip of the cephalosome to the distal lateral end of the last thoracic segment. In addition, body length of euphausiids, amphipods, pteropods, and fish larvae were measured from subsamples of Mulitnet samples taken at stations 8 through 17. Body length of euphausiids and amphipods was measured on stretched animals along the dorsal line from the tip of the rostrum (euphausiids) or the anterior edge of the eye (amphipods) to the tip of the telson. Body length of pteropods was measured as the diameter of their shell. Total length of fish larvae was measure the most forward point of the head to the farthest tip of the tail with the fish lying on its side. Zooplankton density (individuals per m^3) was estimated for each species by stratum by correcting for the mouth-opening area of the net and vertical hauling distance of the statum, assuming 100% filtration efficiency. The weighted mean density estimate for each species per station over the 0-100 m range was calculated using the following equation:

$$\rho = \frac{\sum_{i=1}^{n} \rho^{i} dz^{i}}{\sum_{i=1}^{n} dz^{i}},$$

(Equation 1)

where n is the number of strata, ρ^i is the density of the species in the stratum i in individuals per m^3 (ind. m^{-3}) and dz^i is the thickness of each stratum i in meters.

Macrozooplankton and ichthyoplankton were sampled with a Tucker trawl (1 m^2 opening and 1000 µm mesh size) towed for 15 minutes at 2 knots between 20 to 40 m depth. The targeted depth at each station was determined from the epipelagic SSL identified in the echogram from the vessel's echosounders (Kongsberg Maritime AS, Horten, Norway, www.kongsberg.com; Simrad EK60, 18 and 38 kHz, 1.024 ms pulse duration, 2 Hz pulse repetition). All samples were preserved in a 4% formaldehyde-in-seawater solution buffered with hexamine. Density estimates from the Tucker trawl samples were analysed per station. Each station was sub-sampled using a plankton splitter and counted until at least 300 individuals were identified. The count of each species was extrapolated to the entire sample size and converted to density by accounting for the mount-opening area, deployment speed and time. To document the length distribution of dominant macrozooplankton species captured with the Tucker trawl, random subsamples of euphausiids, amphipods, pteropods and fish larvae were taken from samples of stations 7, 8 and 9 and body length was measured as described above.

For both MultiNet and Tucker trawl samples, species were grouped by taxon. Four taxonomic groups were most abundant: copepods, euphausiid larvae, amphipods, and pteropods. Additionally, fish larvae were included in the analysis because of the high sonar reflectivity of their swimbladder and their socio-economic importance.

III. Acoustic sampling

A. Acoustic data processing

The autonomous hydroacoustic survey was completed using a Sailbuoy equipped with a WBT Mini (Kongsberg Maritime AS) with a 333 kHz transducer (ES333-7CDK splitbeam) operating in broadband mode (283-383 kHz, 1.024 ms pulse duration, 0.5 Hz pulse repetition, fast ramping) for 5 minutes every half hour. The transducer was mounted on the bottom of the Sailbuoy keel at 0.5 m depth. The Sailbuoy keel was always in the water and the transducer was always submerged. Echosounder calibration was performed before the deployment and after the retrieval with a 22.0 mm tungsten carbide (6% cobalt binding) calibration sphere (Demer et al., 2015). Broadband calibration parameters were calculated with the EK80 calibration wizard (version 2.0.1, EK80 software, Kongsberg Maritime AS), and the parameter values were linearly interpolated over the inhibition bands that covered the nulls. Data were calibrated and processed in Echoview (version 12.1, Echoview Software Pty Ltd, Hobart, Australia, www.echoview.com). The maximum range for the analysis was set to 50 m (50.5 m depth) because the signal to background noise ratio diminished below 10 dB (for a signal of -70 dB) at greater ranges.

B. Sound scattering layer backscatter spectra

Sound scattering layers forming discrete horizontal bands of backscatter above the background noise (Proud et al., 2015) were identified using k-means clustering, an unsupervised machine learning algorithm (Lloyd, 1982). Each raw data file output from the echosounder was converted into a netCDF4 file with the open-source software echopype (version 0.5.3; Lee et al., 2021; Figure 2a). Data analysis was restricted to the region between the near-field (3 m range) and the signal-to-noise ratio limit (50 m range). In all echograms, a maximum of one SSL was detected by the clustering algorithm in the upper 50.5 m of the water column. The SSL varied in strength, thickness, and depth. The pulse-compressed volume backscattering strength (S_v in dB re 1m^{-1}) averaged over the frequency spectrum was pre-processed with a mean filter to smooth the backscatter in time (35 pings; or 70 s) and depth (15 bins; or 0.09 m) (Figure 2b). The pre-processing filter revealed the SSL on the depth/S_v projection, as shown in the comparison between the unfiltered data in Figure 2c and the filtered data in Figure 2d.

After the pre-processing, we applied k-means clustering on the depth/S_v dimensions of each data file (between 3 to 5 minutes of data, depending on the file size). The k-means clustering algorithm categorises all the data points into different groups (i.e., clusters). The only parameter adjusted for each SSL was the number of clusters. The other k-means parameters stayed the same for each iteration (k-mean++ initialisation, 10 separate runs, tolerance of $1e^{-4}$, and a maximum of 300 iterations). Selecting the optimal number of clusters is an intrinsic challenge with k-means clustering. Here, the number of clusters was optimal when the entire SSL was grouped into one of the clusters. The SSLs were easier to delineate by clustering when they were thick, had a high S_v and had a distinct separation from surface bubbles or entrained air (Anderson et al., 2007). We typically selected between 3-7 clusters. For example, in Figure 2d where Cluster 0 corresponds to the SSL, we chose to separate the backscatter profile into 3 clusters because of the relatively high S_v within the SSL (i.e., strong backscatter in the SSL relative to the background level).

The upper and lower boundaries of the SSLs identified by the clustering algorithm were imported to Echoview as editable line files to delineate SSL regions (e.g., red lines in Figure 2a which delimit the upper and lower boundaries of the SSL associated with Cluster 0). The broadband spectra of pulse-compressed volume backscattering strength ($S_V(f)$) was extracted from each identified SSL using Echoview's "Wideband Frequency Response" export option. Broadband frequency response values were converted to the linear domain (volume backscattering coefficient spectra, $s_V(f)$). We selected a Fourier transform window size of 0.4 m at a frequency resolution of 100 Hz over the entire bandwidth for a total of 1001 values per SSL. The Fourier transform window size was selected as a compromise between high frequency resolution and a high range resolution (Benoit-Bird and Waluk, 2020). The median and the interquartile range of $s_V(f)$ from each SSL were calculated for further analysis.

C. Sound scattering models

We ran scattering model ensembles per taxonomic group to calculate the theoretical backscatter for the forward and inverse acoustic density estimates. The taxonomic groups were selected from the net and trawl density data.

1. Weakly scattering fluid-like zooplankton

The weakly scatterers were copepods, euphausiid larvae, and amphipods, which were modelled using a prolate spheroid for the copepods and a finite uniformly-bent cylinder for the euphausiid larvae and amphipods. Weakly scatterers have a sound speed contrast *(h)* and density contrast *(g)* of 1 ± 5%. A near-unity sound speed and density contrast implies that the material properties of the scatterers are not significantly different from the surrounding medium (seawater). We chose the phase-compensated distorted wave Born approximation (PC-DWBA) model for the weakly scatterers in our domain because it is specifically adapted to densely aggregated zooplankton (Chu and Ye, 1999). Also, the PC-DWBA is adequate for the range of fluid-like taxonomic groups in the Tromsøflaket epipelagic layer because the parameters are flexible to geometry, material properties, and acoustic frequency changes (Chu and Ye, 1999; Gastauer et al., 2019). We identified the most abundant species of each taxonomic group to determine the model parameters. Copepods were modelled as *Calanus finmarchicus copepodite stage V (CV)* (61% of copepods in the MultiNet samples, Supplementary Materials Table S1), euphausiid larvae were modelled as *Thyssanoessa inermis* (100% of euphausiid larvae in the Tucker Trawl samples, Supplementary Materials Table S2) and amphipods were modelled as *Themisto abyssorum* (100% of amphipods in the MultiNet samples, Supplementary Materials Table S1). We ran 1000 model simulations for each taxonomic group using the ZooScatR package (version 0.5; Gastauer et al., 2019) with varying shape, size, and material properties parameters. These parameters were selected based on literature or net and trawl samples (Table 2). The length distribution for euphausiid larvae was calculated using the measurements of *Thyssanoessa inermis* in the Tucker trawl subsamples from stations 7, 8 and 9 (Figure 1). The length distribution for amphipods was identified by pooling measurements of *Themisto abyssorum* in MultiNet samples from stations 8-17 and Tucker Trawl samples from stations 7, 8 and 9. We repeated 1000 model simulations with random sampling within the distribution of each model parameter (Table 2) to calculate the variance in the cross-sectional backscatter across the available frequency spectrum (283-383 kHz) of each weakly scattering taxonomic group.

2. Elastic-shelled zooplankton

The pteropod taxonomic group was modelled (in Python version 3.7) with a viscous-elastic model (Feuillade and Nero, 1998), as updated by Khodabandeloo et al. (2021). The model is developed for shapes with four layers: gas layer (swimbladder), thin elastic layer (swimbladder wall), thicker viscous layer (fish flesh) and the surrounding medium (seawater). We adjusted the model for pteropods by reducing the thickness of the viscous layer to zero, increasing the thickness of the elastic layer to correspond with the shell thickness, and characterising the gas layer with the material properties of internal soft tissue. The adjustments to the boundary conditions fitted with the literature description of pteropods, a roughly spherical hard aragonite elastic shell with soft and weakly reflecting internal tissue inside (Lavery et al., 2007; MacLennan and Simmonds, 2008). The model is parameterised by the material properties and size of each layer, including the shape (thickness), density and sound speed properties (Khodabandeloo et al., 2021). As with the weakly scatterers, we identified the most abundant species to represent the taxonomic group in the scattering model. The pteropods were modelled as *Limacina retroversa* (100% of pteropods in the Tucker trawl samples, Supplementary Materials Table S2). We assumed a spherical target for the scattering model. To account for the slightly elongated shape, we determined the radii distributions using both the width and length of the subsampled *Limacina retroversa* from the Tucker Trawl samples at stations 7, 8 and 9. The other shape parameters (radius of viscous layer and radius of gas layer; parameterised as a dense fluid layer) were calculated for each ensemble based on the selected elastic shell radius (Table 3). The outer layer was parameterised as aragonite. The internal layer was parameterised as a dense fluid representing the internal tissue with g = 1.022 and h = 1.04 (Lavery et al., 2007). The variance from the parameter space of the viscous-elastic model was assessed by repeating 1000 model iterations with random sampling within the distribution of the radius of the elastic shell parameter (Table 3).

3. Gas-bearing organisms

The fish larvae taxonomic group was modelled with the viscous-elastic model as juvenile/larvae of *Gadus morhua* (70% of fish larvae in the Tucker Trawl, Supplementary Materials Table S2). The main scattering component of a gas-bearing organism is the gas enclosure, in this case the swimbladder. The radius of the elastic shell, the swimbladder including the swimbladder wall, was calculated by converting total length measurements to swimbladder length using relationships from juvenile and larval *Gadus morhua* studied by Chu et al., 2003 (Supplementary Materials Figure S1). The corresponding swimbladder widths were also calculated through a swimbladder length-to-volume linear relationship, assuming a prolate spheroid swimbladder shape (Chu et al., 2003). The viscous-elastic model comparison of a sphere and a prolate spheroid at a range of incident angles indicates that the magnitude of the frequency response is dependent on the local radius at the angle of incidence (Figure 10 in Khodabandeloo et al., 2021). The peaks and nulls are horizontally translated, but these are eliminated through averaging for the volume backscatter of an aggregation. Therefore, we assumed a spherical target and determined the distribution of radii of the fish larvae using swimbladder length and width (R3 in Table 3). The radii distributions were determined from the measured juvenile/larvae *Gadus morhua* from the Tucker Trawl samples at stations 7, 8 and 9.

The other shape parameters (radius of the viscous layer and the gas layer) were calculated for each model simulation iteration based on the randomly selected elastic shell radius (Table 3). The variance from the parameter space of the viscous elastic model was assessed by repeating 1000 model iterations with a random selection of parameters given the distributions in Table 3.

D. Density estimates

The acoustic density estimates are based on the linearity principle that the total scattered energy from a volume is equal to the sum of the scattered energy of each randomly distributed individual scatterers within that volume (Foote, 1983; Greenlaw, 1979; Lavery et al., 2007), given by:

$$s_v(f) = \sum_{i=1}^{N} \sigma_{bs}^{i}(f) * \rho^{i}$$

(Equation 2)

Where $s_v(f)$ is the volume backscattering coefficient spectra in m^2 per m^3 with measurements at all frequencies f in Hz, N is the number of taxonomic groups in the sampled volume, $\sigma^i_{bs}(f)$ is the cross-sectional backscatter spectra of a given taxonomic group i at all frequencies f in m^2, and ρ^i is the density in individuals per m^3 (ind. m^{-3}) for each taxonomic group i.

Estimates based on this equation assume that the entire volume backscatter is formed by the species or taxonomic groups included in the cross-sectional backscatter term. For the forward and inverse methods, we assumed the intensity of the backscattered signal was solely from the five modelled taxonomic groups.

1. Forward method

The forward method is an approach to calculate density or biomass estimates of taxonomic groups from hydroacoustic-trawl survey data (Love, 1975; Davison et al., 2015; Dornan et al., 2022). The forward method for density estimates, as described in MacLennan and Simmonds, 2008, was computed at the nominal frequency (333 kHz) to emulate the results from a narrowband (single frequency) survey, which simplifies Equation 2 to:

$$s_v = \langle \sigma_{bs} \rangle * \rho^{total}$$

(Equation 3)

where s_v is the volume backscattering coefficient at a given frequency, $\langle \sigma_{bs} \rangle$ is the average predicted cross-sectional backscatter weighted by the relative density from net and trawl sampling, and ρ^{total} is the total density in individuals per m^3 (ind. m^{-3}).

We extracted the median s_v at the nominal frequency from the median $s_v(f)$ of each SSL. From the scattering model simulations for each taxonomic group, we extracted the weighted average $\langle \sigma_{bs} \rangle$ at the nominal frequency. The weights were calculated by the mean of the relative densities from the MultiNet and Tucker trawl samples (Supplementary Materials Table S3 and Table S4). The calculated ρ^{total} for each SSL was divided among the taxonomic groups based on the relative density.

2. Inverse method

Alternatively, the inversion of the broadband scattering data can be used to solve Eq. 1 with a least-squares data fitting solver, as in Lavery et al., 2010 (Greenlaw, 1979; Lavery et al., 2007). From the scattering model simulations for each taxonomic group, we calculated the median cross-sectional backscatter, $\sigma^i_{bs}(f)$ (Eq. 2) and 90%

bootstrap interval of the median across the frequency spectrum. To calculate the density of each taxonomic group for the autonomous hydroacoustic survey with the inverse method, we solved Equation 2 for density ρ^i as a linear least-squares problem by using a Trust Region Reflective algorithm as described in Branch et al. (1999). The optimiser (Python version 3.7, scipy.optimise.lsq_linear) determined the best solution by minimising the following problem with the following bounds (0 <= ρ^i < inf.):

$$0.5 * \left|\left|\sigma_{bs}^{i}(f) \ * \ \rho^{i} - s_{v}(f),\right|\right|^{2}$$

(Equation 4)

A sensitivity analysis was conducted to quantify the effect of altering species shape and material properties on the variability of the inverse method density estimates. We ran 500 random permutations of Eq. 3 with replacement. The cross-sectional backscatter spectra of each species varied between the median, the 5th and 95th percentiles. The $s_v(f)$ of each SSL varied between the median and the interquartile range.

IV. Comparison analysis

For comparison across all four methods, we performed a Kruskal-Wallis *H* test. For non-parametric pairwise comparisons, Dunn's tests were computed with p-values adjusted with the Benjamini-Hochberg adjustment (non-negative) to assess the significance of the difference in density estimates between each method pair for each taxonomic group.

Results

I. Biological sampling

Copepods dominated the mesozooplankton community sampled with the MultiNet with a mean density with standard error (± SE) of 1800 ± 300 ind. m^{-3} (95% of the density, Figure 3). Pteropods were the second most abundant taxonomic group in the MultiNet samples, with a mean density of 50 ± 30 ind. m^{-3}. Euphausiid larvae had a low density (9 ± 2 ind. m^{-3}, 0.5% of the community); most of these were represented by euphausiid larvae in *furcilia* stages (89% of euphausiid larvae over all MultiNet samples). Other species, such as siphonophores and meroplankton, not included in the selected taxonomic group for this study, accounted for 30 ± 5 ind. m^{-3}, or 2%, of the MultiNet catch in the study region. Detailed MultiNet density data are presented in Supplementary Materials Table S1 and Table S3.

Like the MultiNet samples, the Tucker trawl samples were primarily composed of copepods (54% of the community, Figure 4), but the average density was much lower with 19 ± 5 ind. m^{-3} (Figure 3). Small pteropods (mean length = 1.2 mm, Table 4) were the second most abundant taxonomic group in the trawl samples, with a mean density of 5 ± 1 ind. m^{-3} (17% of the community). Euphausiid larvae had comparable density (3.5 ± 0.7 ind. m^{-3}, 16% of the community); most of these larvae were *Thyssanoessa inermis* (99.8% of euphausiid larvae in the Tucker Trawl sample). The mean length of the larvae was 4.7 mm suggesting they were still young of the year, like the furcilia stages from the MultiNet samples (mean length 4.0 mm; Table 4). Other species not included in the selected taxonomic group for this study, such as siphonophores and decapod crustaceans, accounted for 7% of the Tucker trawl catch in the study region. Detailed Tucker trawl density data are available in Supplementary Materials Table S2 and Table S4.

II. Acoustics

A. Sound scattering layer detection

The k-means clustering algorithm identified a total of 70 SSLs over the autonomous acoustic survey period. The SSLs varied between 1 m to 29 m (min. and max.) in thickness, with the layers centred at an average depth of 20.6 m. The median volume backscattering strength spectra from all the SSLs varied between -75 to -50 dB re 1 m^{-1} (min. and max.). At the nominal frequency, the median *Sv (f)* varied between -73 and -56 dB re 1 m^{-1} (min. and max.).

B. Scattering models

The target strength (TS) frequency response varied in strength and shape across the taxonomic groups. The median broadband TS ranged from a minimum of -100 dB re 1 m^2 at the lowest frequency, 283 kHz, for the smallest fluid-like weakly scatterer, copepod taxonomic group, to a maximum of -65 dB re 1 m^2 at 345 kHz from the gas-bearing taxonomic group, fish larvae (Figure 5). Copepods, euphausiid larvae and fish larvae TS spectra had a positive slope with TS increasing with frequency, whereas amphipods and pteropods had a negative sloping TS(f) (Supplementary Materials Figure S2, shown as cross-sectional backscatter spectra, i.e., linear form of TS). The cross-sectional backscatter matrix had a rank of 5, suggesting the taxonomic groups were linearly independent and can be distinguished by the least-squares algorithm.

C. Forward method density estimates

Based on the relative density results from the MultiNet and Tucker trawl, the forward method estimated SSLs dominated by copepods (56 ± 6 ind. m^{-3}) followed by pteropods (7.0 ± 0.7 ind. m^{-3}), euphausiid larvae (4.3 ± 0.5 ind. m^{-3}), amphipods (1.6 ± 0.2 ind. m^{-3}) and fish larvae (0.40 ± 0.04 ind. m^{-3}) (Figure 3). The relative density was a fixed input parameter in the calculation; therefore, the forward method was not included in Figure 4.

D. Inverse method density estimates

The density estimates measured from the inversion of the autonomous acoustic survey showed an SSL dominated by the copepods (3700 ± 200 ind. m^{-3}; 77% of acoustic density estimates), which agreed with the MultiNet results. The second most abundant group in the acoustic results was euphausiid larvae (modelled as *Thyssanoessa inermis* from Tucker trawl), with 1300 ± 200 ind. m^{-3}, representing 23% of the total taxonomic composition. In the inverse method estimates, amphipods had a higher density than pteropods with 10.3 ± 0.5 ind. m^{-3} (0.2%) and 3.9 ± 0.2 ind. m^{-3} (0.08%), respectively. The fish larvae had the lowest density as with the other sampling methods, 0.126 ± 0.001 ind. m^{-3}; 0.002% of the total composition.

The sensitivity analysis showed the variability in the density estimates compared to the variation in the model parameters and the volume backscatter within each SSL (standard deviation). The sensitivity of density estimates was compared to the distribution of densities of the 70 SSLs. For the copepods and euphausiid larvae, the effect of the dispersion in the model parameters and volume backscatter variability was smaller than the standard deviation from the density estimates of all the SSLs (Figure 6 a, b). Conversely, amphipods, fish larvae and pteropods density estimates had a larger sensitivity to the model parameters and volume backscatter than the variability in density estimates across the study region (Figure 6 c, d, e). Density estimates of all species showed higher variability in the case of SSLs with high backscatter (e.g., SSL n˚ 47-48; Figure 6).

III. Density analysis across methods

All four methods compared in this analysis (MultiNet, Tucker trawl, and forward and inverse method with autonomous acoustic survey data) showed that copepods dominated the epipelagic SSL across the study area (> 50% density for all sampling methods, Figure 4). However, comparisons of density estimates for all methods were significantly different for each taxonomic group as revealed by a Kruskal-Wallis *H* test, denoted with degrees of freedom in parenthesis (copepods: $H(3) = 127.87$, $p<0.0001$; euphausiid larvae: $H(3) = 121.24$, $p<0.0001$; amphipods: $H(3) = 115.14$, $p<0.0001$; fish larvae: $H(3) = 118.10$, $p<0.0001$; pteropods: $H(3) = 31.89$, $p<0.0001$) (Figure 3).

Density estimates were significantly different between the MultiNet and Tucker trawl for copepods, pteropods, and fish larvae (Dunn's test; $p<0.01$). No significant differences in density estimates between the net and trawl were found for the other taxonomic groups (euphausiid larvae: $p=0.19$ and amphipods: $p=0.79$). Results from pairwise comparisons from Dunn's tests are shown in Figure S3 (in Supplementary Materials). Density estimates of euphausiid larvae were almost three times higher based on the MultiNet samples than the Tucker trawl samples. However, the relative density of euphausiid larvae in the Tucker trawl samples was higher (11.1%) than in the MultiNet samples (0.5%) (Figure 4). As with the euphausiids, pteropods density was eleven times higher in the MultiNet samples than in the Tucker trawl samples, but pteropods had a lower relative density in the MultiNet (2.8% of the community) than in the Tucker Trawl (16.1%). For amphipods, similar densities were sampled by net and trawl (1.2 ± 0.3 ind. m^{-3} for MultiNet and 1.4 ± 0.3 ind. m^{-3} for Tucker trawl). Fish larvae were found in low densities, on average 0.05 ± 0.02 ind. m^{-3} in the MultiNet and 0.3 ± 0.2 ind. m^{-3} in the Tucker trawl, and had low relative densities in both net and trawl (<1% of the total catch in both direct sampling methods).

A pairwise comparison of the forward method for acoustic data analysis showed that these density estimates were not statistically different from the Tucker trawl estimates for all taxonomic groups (copepods: $p=0.08$; euphausiid larvae: $p=0.77$; amphipods: $p=0.79$; fish larvae: $p=0.31$; pteropods: $p=0.07$). In contrast, density estimates from the forward method were statistically different from estimates from the MultiNet samples for copepods ($p<0.01$), fish larvae ($p<0.001$) and pteropods ($p<0.01$), but not for the euphausiid larvae ($p=0.18$) and amphipods ($p=0.76$). The density estimates calculated from the autonomous acoustic survey data by the forward and inverse methods were statistically different for all taxonomic groups ($p<0.01$).

Pairwise comparisons indicated that the autonomous acoustic survey density estimates calculated through inversion differed significantly from the other sampling methods for the euphausiid larvae and amphipods (Dunn's test; $p<0.001$). However, for the copepods, the inverse results were not statistically different from the MultiNet ($p=0.06$) but statistically different from Tucker trawl ($p<0.001$). The results from the inverse method were not statistically different from densities measured from the Tucker trawl for pteropods ($p=0.92$) but were statistically different from the results of the MultiNet and forward method ($p<0.01$). For fish larvae, the densities measured from the MultiNet were not statistically different from the results of the inverse method ($p=0.58$) but were statistically different from the densities measured from the Tucker trawl and forward method ($p<0.001$).

Overall, the inverse method reported the highest total average density of 4987 ind. m^{-3}, followed by the MultiNet samples (1931 ind. m^{-3}), the forward method (70 ind. m^{-3}) and the Tucker trawl samples (29 ind. m^{-3}).

Discussion

I. Comparison of sampling methods

To our knowledge, this study is one of the first implementations of the inverse method from an autonomous broadband acoustic survey with TS estimates informed by locally derived measurements of shape properties. The inverse method yielded higher density estimates. These density estimates are most likely a more accurate representation of the sound scattering layers for the five dominant plankton taxonomic groups in the Norwegian Sea. Net and trawl sampling likely underestimated zooplankton densities within the SSL because of gear-specific biases when assessing species composition across size classes (Skjoldal et al., 2013; Hetherington et al., 2022).

All sampling methods determined that copepods dominated the epipelagic SSL in Tromsøflaket. The relative density of copepods calculated from the inverse method (77%) was between the MultiNet (95%) and Tucker trawl (54%). We suspect that because the copepods were relatively large individuals (mainly *Calanus finmarchicus CV* with a mean length of 2.6 mm) organised in dense swarms, the high frequency and high bandwidth (283-383 kHz) of the acoustic instrument detected most of these copepods. The agreement of the density estimates from the inverse method and MultiNet suggests that the high vertical resolution of the broadband acoustic data could be used to increase the accuracy of copepod density estimates within the epipelagic layer. In the future, satellite observations of ocean colour could compensate for the blind zone of acoustic measurements near the surface and measure the near-surface density of copepods (Basedow et al., 2019).

Variations in organism size and swimming abilities must be considered when designing surveys and selecting sampling methods. The MultiNet targets small zooplankton species (>0.3 mm), especially weak swimmers aggregating in high densities. The Tucker trawl is designed to catch larger, fast-swimming zooplankton and ichthyoplankton species in the epipelagic layer. Therefore, we did not expect to find higher densities of euphausiid larvae in the MultiNet compared to the Tucker trawl since they are known to avoid MultiNets and similar gear (Brinton, 1967; Greenlaw, 1979). The inverse method estimated densities of euphausiid larvae as more than 100 times higher than the net, trawl, and forward method. Because of the well-known ability of euphausiids to avoid capture by standard oceanographic nets (Wiebe et al., 1982), we suggest that the density estimates of euphausiid larvae based on the inverse method are likely closer to reality than the estimates based on the compared methods. Both the MultiNet and Tucker trawl captured small euphausiids (mean length in MultiNet = 4.0 mm and mean length in Tucker trawl = 4.7 mm, Table 4), which did not have the backscattering properties of adults. Young euphausiids have less than 30% of the lipid content of adults, which reduces their density contrast (Kögeler et al., 1987). We expect the density difference of the net, trawl, and forward method to the inverse method to be even larger in the case of adult euphausiids because of their increased avoidance abilities and stronger sound scattering properties.

The relatively high densities of both small (copepods) and larger mobile (amphipods and euphausiids) zooplankton measured with the inverse method suggests that this approach can accurately sample a larger size spectrum of targets than the other methods. Similar to euphausiids, density estimates of amphipods were higher when calculated with the inverse method. Amphipods are also fairly strong scatterers and mobile swimmers (Skjoldal et al., 2013). We conclude that the inverse method from autonomous acoustic surveys provided the best density estimates for agile organisms that avoid nets and trawls.

The inverse acoustic method could be applied to larger organisms than zooplankton, such as pelagic fish. Sampling efficiency for fish and their vertical distribution in the water column has been widely studied because of the socio-economic importance of fisheries (Handegard and Tjøstheim, 2005). A net comparison study from June 1993 in Storfjorden, Norway, has reported a higher density of ichthyoplankton between 50-100 m than between 0 – 50 m (Skjoldal et al., 2013). The autonomous acoustic monitoring system used in this study had a maximum depth of 50.5 m, limiting the detection of fish larvae in deeper regions of the epipelagic layer. Yet, ichthyoplankton densities were comparable between methods. One way of improving estimates of density and vertical distribution pattern of fish larvae in high latitude shelf areas could be to use the inverse method with a transducer with a deeper detection range (lower frequency band or longer pulse length) or using both surface and underwater vehicles, such as gliders. A lower frequency bandwidth (for example, 185-255 kHz) would also be beneficial for measuring the density of ichthyoplankton and pteropods because they have a stronger acoustic backscatter at lower frequencies.

Zooplankton layers are known to exhibit patchiness; therefore, variability in relative density across the sampling region is expected (Trevorrow et al., 2005, Basedow et al., 2006, Trudnowska et al., 2016). For example, we found high variability in pteropod densities based on net samples between stations (maximum at station 13 with 379 ind. m^{-3} and minimum at station 17 with 2 ind. m^{-3}), which likely results from their patchy distribution (Elizondo and Vogt, 2022). The Tucker trawl did not capture such a broad variability in densities (maximum at station 8 with 16 ind. m^{-3} and a minimum at station 17 with 0.5 ind. m^{-3}), which may be due to the larger mesh underestimating the small pteropods (mean length of 1.2 mm; Table 4). Because the net and trawl sampling and the acoustic measurements are not coincident in time and space in this study, we used a static average relative density to reflect the species composition of the region. In contrast, the inverse method provides continuous measurements and is not dependant on punctual sampling.

II. Assessment of the autonomous acoustic survey and inverse method for density estimates

Autonomous acoustic surveys require effective data processing methods that limit the introduction of biases and can quickly be applied to large datasets. The results of the k-means clustering algorithm revealed that, despite being ubiquitous over the study area, the sound scattering layer varied in thickness, volume backscattering strength, and depth over time and space. This algorithm restricted the user bias of identifying boundaries and increased reproducibility because the only subjective parameter in this machine learning algorithm was the number of clusters. The successful application of the k-means clustering method for identifying SSLs in the Tromsøflaket area suggests that it can now be tested on more complex vertical structures with multiple discrete SSLs in different regions.

Density estimates were corrected for the sampling volume for each method; however, the differences in sampling depths could influence the results. The acoustic estimates were bounded by the edges of the epipelagic SSLs which were determined by k-mean clustering and typically found between 3.5 – 50 m, whereas the Tucker trawl sampled 0 – 20 or 40 m and the MultiNet sampled 0 – 100 m. The acoustic density estimates did not incorporate volumes with lower densities above and below the epipelagic SSL. In contrast, the densities calculated from nets and trawls were averaged over the entire sampling range. The acoustic inversion was only applicable within the boundaries of the SSL where the density of scatterers is high. If the density of scatterers is too low, the echo statistics are dependent on the target's location in the beam rather than the intensity summation process (Holliday and Pieper, 1995). Under such low-density scenarios, single echo detections and echo counting (Keiser and Mulligan, 1984; Simmonds and MacLennan, 2008) should be used instead of the inverse method. However, if differences in density estimates were driven by differences in sampling depths, we would expect high densities from both acoustic methods, not just the inverse method.

In this study, we relied on the size distribution of the dominant species locally derived from nets and trawls to inform the scattering models because the 283-383 kHz bandwidth only detected the geometric scattering of the targets (ka>1; Lavery et al., 2010). However, with a broader frequency spectrum that captures the Rayleigh-to-geometric scattering transition of all taxa, the size classes can be identified within the inverse method (Greenlaw, 1979; Lavery et al., 2007; Cotter et al., 2021). In that case, the scattering transition point determines the resonance frequency, which is inversely proportional to the size of the scatterers and can increase the ability to differentiate among taxa (Holliday and Pieper, 1995; Warren et al., 2003; Benoit-Bird, 2009). Capturing the Rayleigh-to-geometric transition would thus improve the method because it produces a frequency response curve with a more identifiable shape (Cotter et al., 2021). Nonetheless, we demonstrated that relying on a bandwidth covering the transition point is not necessary to determine the density of epipelagic organisms using the inverse method when size distributions are provided by net and trawl samples.

The sensitivity analysis tested the variability in the frequency-response curves compared to the variability in the model parameters and showed that the density estimates of the stronger scatterers (amphipods, fish larvae and pteropods) had a larger sensitivity to the model parameters than the weaker scatterers (copepods and euphausiid larvae). The inverse method is based on absolute scattering levels, which rely heavily on calibration (Lavery et al., 2007). A two-sphere calibration covering the entire broadband signal should be carefully completed for future density calculations using the inverse method. Careful calibration across the bandwidth is critical, as with multi-frequency analysis, to avoid artificial trends in the frequency-response curves. In addition, the inverse method requires knowledge of the scattering model parameters for each taxonomic group. Here, some of these parameters were informed by the net and trawl data but others were defined based on previous literature values. Variability in model parameters like orientation or material properties can affect the density estimates, especially for the stronger scatterers as shown by the sensitivity analysis. *In situ* measurements of material properties, sound speed, and density contrasts, and more knowledge about the orientation of the scatterers would restrict the variability of model simulation results and improve the accuracy of the density estimates.

Because of their low taxonomic resolution, both the forward and inverse acoustic methods are dependent on the initial taxonomic group selection. Different statistical or data-fitting approaches with an error term could better account for non-dominant species, such as meroplankton and decapod larvae. In the current study, errors in the taxonomic classification would lead to a positive bias in the density estimates from the acoustic methods. The limited taxonomic resolution of the acoustic inversion method could be improved by the addition of imaging sensors which are already being integrated on autonomous platforms equipped with a wideband echosounder (Whitmore et al., 2019; Reiss et al., 2021). Optical sensors could also provide information on the size and, to some extent, the orientation of the scatterers (Ohman et al., 2019), which would improve the *in situ* scattering models.

Conclusion

The inverse method was used to quantify aggregations of zooplankton and ichthyoplankton with a broadband autonomous hydroacoustic survey and detected higher densities of abundant mobile zooplankton than the net, trawl, and forward acoustic method. The inverse method also detected similar densities of smaller mesozooplankton to the net samples. We conclude that it is the most accurate method to measure the density of a broad size spectrum of zooplankton, and most likely of ichthyoplankton and pelagic fish. This work built on studies on the inverse method for zooplankton layers (Lavery et al., 2007), autonomous hydroacoustic surveys (De Robertis et al., 2019) and broadband data processing (Basset et al., 2019, Benoit-Bird and Waluk et al., 2020) in recent years. We further advanced the field by offering a solution for the limitation of sparse coexisting biological sampling from autonomous acoustic surveys by using the inverse method with locally derived size measurements.

Accurate density estimates of pelagic organisms with high spatio-temporal resolution are critical to conducting stock assessment surveys and understanding the impact of changes in the epipelagic zone and their effects on food supply to deeper water ecosystems (Rogers, 2015). To this end, we conclude that applying the inverse method to broadband hydroacoustic data can improve the accuracy of acoustic-trawl surveys. We further envision that applying the inverse method to acoustic data collected from autonomous platforms could supplement and extend the spatial resolution of vessel-based surveys at a lower cost than additional ship time.

Acknowledgement

The authors thank Babak Khodabandeloo and Sven Gastauer for providing scattering model software and advice. Also, we thank Jennifer Herbig for reading and editing an early draft of the manuscript and for her statistical expertise. We acknowledge the valuable comments and suggestions from the reviewers, which helped us to improve the quality of the manuscript.

Author contribution statement

MDu: Conceptualisation, Methodology, Software, Formal Analysis, Visualisation, Writing – original draft

GP: Conceptualisation, Supervision, Writing – review & editing

SB: Investigation, Writing – review & editing

MDa: Conceptualisation, Investigation, Writing – review & editing

SFP: Investigation, Writing – review & editing

LC: Funding Acquisition, Resources

LB: Software, Visualisation

MG: Conceptualisation, Supervision, Writing – review & editing

Funding statement

This research was funded by GLIDER Phase I project, which was funded by the DEMO2000 research program (Norwegian Research Council and ConocoPhillips Skandinavia AS, project no. 269188, "Unmanned ocean vehicles, a flexible and cost-efficient offshore monitoring and data management approach") and by Glider Phase II financed by ConocoPhillips Skandinavia AS. The research survey was funded by "Collaborative Studies of Two Resource Ecosystems in Shelf, Slope an Oceanic Regions of the Norwegian and South China Seas (Stressor)", funded by the Norwegian Research Council (project no. 287043). Maxime Geoffroy's participation is financially supported by the Discovery Grant program of the Natural Science and Engineering Research Council of Canada. Geir Pedersen's participation was co-funded by CRIMAC (Norwegian Research Council project no. 309512).

Competing interests

The authors declare that they have no known competing financial interests or personal relationships that could potentially influence the research reported in this paper.

Data availability statement

Acoustic data generated or analysed during this study are available in the " EK80 raw data collected by autonomous sailbuoy in Lofoten/Vesterålen, 2018-06-18–2018-06-30" repository (https://doi.org/10.5281/zenodo.6786851). Location and other sensor observations from the autonomous surface vehicle data generated or analysed during this study are available in the "Real-time oceanography captured by autonomous sailbuoy in Lofoten/Vesterålen 2018" repository (https://doi.org/10.5281/zenodo.6786919)

References

Andersen, L.N., Chu, D., Heimvoll, H., Korneliussen, R., Macaulay, G.J. and Ona, E., 2021. Quantitative processing of broadband data as implemented in a scientific splitbeam echosounder. arXiv preprint arXiv:2104.07248. doi.org/10.1121/10.0002943

Anderson, C.I.H., Horne, J.K. and Boyle, J., 2007. Classifying multi-frequency fisheries acoustic data using a robust probabilistic classification technique. *The Journal of the Acoustical Society of America*, *121*(6), pp.EL230-EL237. doi.org/10.1121/1.2731016

Appenzeller, A.R. and Leggett, W.C., 1992. Bias in hydroacoustic estimates of fish abundance due to acoustic shadowing: evidence from day–night surveys of vertically migrating fish. *Canadian Journal of Fisheries and Aquatic Sciences*, *49*(10), pp.2179-2189. doi.org/10.1139/f92-240

Bandara, K., Basedow, S.L., Pedersen, G. and Tverberg, V., 2022. Mid-summer vertical behavior of a high-latitude oceanic zooplankton community. *Journal of Marine Systems*, *230*, p.103733. doi.org/10.1016/j.jmarsys.2022.103733

Barham, E.G., 1966. Deep scattering layer migration and composition: observations from a diving saucer. Science, 151(3716), pp.1399-1403. doi.org/10.1126/ science.151.3716.1399w, S.L., Edvardsen, A. and Tande, K.S., 2006. Spatial patterns of surface blooms and recruitment dynamics of Calanus finmarchicus in the NE Norwegian Sea. Journal of plankton research, 28(12), pp.1181-1190. doi.org/10.1093/plankt/fbl048

Basedow, S.L., McKee, D., Lefering, I., Gislason, A., Daase, M., Trudnowska, E., Egeland, E.S., Choquet, M. and Falk-Petersen, S., 2019. Remote sensing of zooplankton swarms. *Scientific reports*, *9*(1), pp.1-10. doi.org/10.1038/s41598-018-37129-x

Bassett, C., Lavery, A.C. and Stanton, T.K., 2019. Broadband measurements of the acoustic target strength of mesopelagic fishes. *The Journal of the Acoustical Society of America*, *146*(4), pp.2772-2772. doi.org/ 10.1121/1.5136601

Battaglia, A., Trenkel, V.M. and Rochet, M.J., 2006. Estimating end effects in trawl catches. *ICES Journal of Marine Science*, *63*(5), pp.956-959. doi.org/10.1016/j.icesjms.2006.03.002

Bellec, V., Wilson, M., Bøe, R., Rise, L., Thorsnes, T., Buhl-Mortensen, L. and Buhl-Mortensen, P., 2008. Bottom currents interpreted from iceberg ploughmarks revealed by multibeam data at Tromsøflaket, Barents Sea. *Marine Geology*, *249*(3-4), pp.257-270. doi.org/10.1016/j.margeo.2007.11.009

Benoit-Bird, K.J. and Waluk, C.M., 2020. Exploring the promise of broadband fisheries echosounders for species discrimination with quantitative assessment of data processing effects. *The Journal of the Acoustical Society of America*, 147(1), pp.411-427. doi.org/10.1121/10.0000594

Benoit-Bird, K.J., 2009. The effects of scattering-layer composition, animal size, and numerical density on the frequency response of volume backscatter. *ICES Journal of Marine Science*, *66*(3), pp.582-593. doi.org/10.1093/icesjms/fsp013

Berge, J., Geoffroy, M., Daase, M., Cottier, F., Priou, P., Cohen, J.H., Johnsen, G., McKee, D., Kostakis, I., Renaud, P.E. and Vogedes, D., 2020. Artificial light during the polar night disrupts Arctic fish and zooplankton behaviour down to 200 m depth. *Communications biology*, *3*(1), pp.1-8. doi.org/10.1038/s42003-020-0807-6

Blanluet, A., Doray, M., Berger, L., Romagnan, J.B., Le Bouffant, N., Lehuta, S. and Petitgas, P., 2019. Characterisation of sound scattering layers in the Bay of Biscay using broadband acoustics, nets and video. *PloS one*, *14*(10), p.e0223618. doi.org/10.1371/journal.pone.0223618

Branch, M. A., Coleman, T. F., & Li, Y. 1999. A subspace, interior, and conjugate gradient method for large-scale bound-constrained minimisation problems. *SIAM Journal on Scientific Computing*, *21*(1), 1-23. doi.org/10.1137/s1064827595289108

Brinton, E., 1967. Vertical migration and avoidance capability of euphausiids in the California Current. *Limnology and Oceanography*, *12*(3), pp.451-483. doi.org/10.4319/lo.1967.12.3.0451

Camus, L., Pedersen, G., Falk-Petersen, S., Dunlop, K., Daase, M., Basedow, S.L., Bandara, K., Tverberg, V., Pederick, J., Peddie, D. and Langeland, T., 2019. Autonomous surface and underwater vehicles reveal new discoveries in the Arctic Ocean. *OCEANS 2019-Marseille*, pp.1-8. doi.org/10.1109/oceanse.2019.8867089

Chu, D. and Wiebe, P.H., 2005. Measurements of sound-speed and density contrasts of zooplankton in Antarctic waters. *ICES Journal of Marine Science*, *62*(4), pp.818-831.

Chu, D., and Ye, Z. 1999. A phase-compensated distorted wave born approximation representation of the bistatic scattering by weakly scattering objects: Application to zooplankton. *The Journal of the Acoustical Society of America*, *106*(4), 1732-1743. doi.org/10.1016/j.icesjms.2004.12.020

Chu, D., Wiebe, P.H., Copley, N.J., Lawson, G.L. and Puvanendran, V., 2003. Material properties of North Atlantic cod eggs and early-stage larvae and their influence on acoustic scattering. *ICES Journal of Marine Science*, 60(3), pp.508-515. doi.org/10.1016/s1054-3139(03)00047-x

Cotter, E., Bassett, C. and Lavery, A., 2021. Classification of broadband target spectra in the mesopelagic using physics-informed machine learning. *The Journal of the Acoustical Society of America*, 149(6), pp.3889-3901. doi.org/10.1016/s1054-3139(03)00047-x

Davison, P.C., Koslow, J.A. and Kloser, R.J., 2015. Acoustic biomass estimation of mesopelagic fish: backscattering from individuals, populations, and communities. *ICES Journal of Marine Science*, *72*(5), pp.1413-1424. doi.org/10.1093/icesjms/fsv023

De Robertis, A., Wilson, C.D. and Williamson, N.J., 2012. Do silent ships see more fish? Comparison of a noise-reduced and a conventional research vessel in Alaska. In *The Effects of Noise on Aquatic Life* (pp. 331-334). Springer, New York, NY. doi.org/10.1007/978-1-4419-7311-5_74

De Robertis, A., Lawrence-Slavas, N., Jenkins, R., Wangen, I., Mordy, C.W., Meinig, C., Levine, M., Peacock, D. and Tabisola, H., 2019. Long-term measurements of fish backscatter from Saildrone unmanned surface vehicles and comparison with observations from a noise-reduced research vessel. *ICES Journal of Marine Science*, 76(7), pp.2459-2470. doi.org/10.1093/icesjms/fsz124

Demer, D.A. and Hewitt, R.P., 1995. Bias in acoustic biomass estimates of Euphausia superba due to diel vertical migration. *Deep Sea Research Part I:*

Oceanographic Research Papers, *42*(4), pp.455-475. doi.org/10.1016/0967-0637(94)e0005-c

Demer, D.A., Berger, L., Bernasconi, M., Bethke, E., Boswell, K., Chu, D., Domokos, R., Dunford, A., Fassler, S., Gauthier, S. and Hufnagle, L.T., 2015. Calibration of acoustic instruments. doi.org/10.23919/oceans40490.2019.8962778

Dietz, R.S., 1948. Deep scattering layer in the Pacific and Antarctic Oceans. *Journal of marine research*, 7(3), pp.430-442.

Dornan, T., Fielding, S., Saunders R.A. and Genner, M.J., 2022. Large mesopelagic fish biomass in the Southern Ocean resolved by acoustic properties. *Proceedings of the Royal Society B*, *289*(1967), p.20211781. https://doi.org/10.1098/rspb.2021.1781

Elizondo, U.H. and Vogt, M., 2022. Individual-based modeling of shelled pteropods. *Ecological Modelling, 468*, p.109944. doi.org/10.1016/j.ecolmodel.2022.109944

Falk-Petersen, S., Gatten, R.R., Sargent, J.R. and Hopkins, C.C.E., 1981. Ecological investigations on the zooplankton community in Balsfjorden, Northern Norway: seasonal changes in the lipid class composition of *Meganyctiphanes norvegica* (M. Sars), *Thysanoessa raschii* (M. Sars), and *T. inermis* (Krøyer). *Journal of*

Experimental Marine Biology and Ecology, *54*(3), pp.209-224. doi.org/10.1016/0022-0981(81)90158-1

Falk-Petersen, S. and Kristensen, Å., 1985. Acoustic assessment of krill stocks in Ullsfjorden, north Norway. *Sarsia*, *70*(1), pp.83-90. doi.org/10.1080/00364827.1985.10420620

Feuillade, C. and Nero, R.W., 1998. A viscous-elastic swimbladder model for describing enhanced-frequency resonance scattering from fish. *The Journal of the Acoustical Society of America*, *103*(6), pp.3245-3255. doi.org/10.1121/1.423076

Foote, K.G., 1983. Linearity of fisheries acoustics, with addition theorems. The Journal of the Acoustical Society of America, 73(6), pp.1932-1940. doi.org/10.1121/1.389583

Gastauer, S., Chu, D. and Cox, M.J., 2019. ZooScatR—An r package for modelling the scattering properties of weak scattering targets using the distorted wave Born approximation. *The Journal of the Acoustical Society of America*, *145*(1), pp.EL102-EL108. doi.org/10.1121/1.5085655

Gjøsæter, H., Ingvaldsen, R. and Christiansen, J.S., 2020. Acoustic scattering layers reveal a faunal connection across the Fram Strait. *Progress in Oceanography*, *185*, p.102348. doi.org/10.1016/j.pocean.2020.102348

Greenlaw, C.F., 1979. Acoustical estimation of zooplankton populations 1. *Limnology and Oceanography*, *24*(2), pp.226-242. doi.org/10.4319/lo.1979.24.2.0226

Handegard, N.O. and Tjøstheim, D., 2005. When fish meet a trawling vessel: examining the behaviour of gadoids using a free-floating buoy and acoustic split-beam tracking. *Canadian Journal of Fisheries and Aquatic Sciences*, 62(10), pp.2409-2422. doi.org/10.1139/f05-131

Holliday, D.V., 1977. Extracting bio-physical information from the acoustic signature of marine organisms. *Oceanic sound scattering prediction*, pp.619-624.

Holliday, D.V. and Pieper, R.E., 1995. Bioacoustical oceanography at high frequencies. *ICES Journal of Marine Science*, *52*(3-4), pp.279-296. doi.org/10.1016/1054-3139(95)80044-1

Hetherington, E.D., Choy, C.A., Thuesen, E.V. and Haddock, S.H., 2022. Three Distinct Views of Deep Pelagic Community Composition Based on Complementary

Sampling Approaches. *Frontiers in Marine Science*, *9*.
doi.org/10.3389/fmars.2022.864004

Jech, J.M., Horne, J.K., Chu, D., Demer, D.A., Francis, D.T., Gorska, N., Jones, B., Lavery, A.C., Stanton, T.K., Macaulay, G.J. and Reeder, D.B., 2015. Comparisons among ten models of acoustic backscattering used in aquatic ecosystem research. *The Journal of the Acoustical Society of America*, *138*(6), pp.3742-3764.
doi.org/10.1121/1.4937607

Kędra, M., Renaud, P.E. and Andrade, H., 2017. Epibenthic diversity and productivity on a heavily trawled Barents Sea bank (Tromsøflaket). *Oceanologia*, *59*(2), pp.93-101.
doi.org/10.1016/j.oceano.2016.12.001

Kieser, R., and Mulligan, T. J., 1984. Analysis of echo counting data: a model. *Canadian Journal of Fisheries and Aquatic Sciences*, *41*(3), pp.451-458.
doi.org/10.1139/f84-054

Khodabandeloo, B., Agersted, M.D., Klevjer, T., Macaulay, G.J. and Melle, W., 2021. Estimating target strength and physical characteristics of gas-bearing mesopelagic fish from wideband in situ echoes using a viscous-elastic scattering model. *The Journal of the Acoustical Society of America*, *149*(1), pp.673-691. doi.org/10.1121/10.0003341

Knutsen, T., Wiebe, P.H., Gjøsæter, H., Ingvaldsen, R.B. and Lien, G., 2017. High latitude epipelagic and mesopelagic scattering layers—A reference for future Arctic ecosystem change. *Frontiers in Marine Science*, *4*, p.334. doi.org/10.3389/fmars.2017.00334

Kögeler, J.W., Falk-Petersen, S., Kristensen, Å., Pettersen, F. and Dalen, J., 1987. Density-and sound speed contrasts in sub-Arctic zooplankton. *Polar Biology*, *7*(4), pp.231-235. doi.org/10.1007/bf00287419

Lavery, A.C., Wiebe, P.H., Stanton, T.K., Lawson, G.L., Benfield, M.C. and Copley, N., 2007. Determining dominant scatterers of sound in mixed zooplankton populations. *The Journal of the Acoustical Society of America*, *122*(6), pp.3304-3326. doi.org/10.1121/1.2793613

Lavery, A.C., Chu, D. and Moum, J.N., 2010. Measurements of acoustic scattering from zooplankton and oceanic microstructure using a broadband echosounder. *ICES Journal of Marine Science*, *67*(2), pp.379-394. doi.org/10.1093/icesjms/fsp242

Lee, W.J., Staneva, V., Mayorga, E., Nguyen, K., Satiewan, L. and Majeed, I., 2021. Echopype: Enhancing the interoperability and scalability of ocean sonar data processing. *The Journal of the Acoustical Society of America*, *149*(4), pp.A63-A63. doi.org/10.1121/10.0004522

Love, R.H., 1975. Predictions of volume scattering strengths from biological trawl data. *The Journal of the Acoustical Society of America*, *57*(2), pp.300-306. doi.org/10.1121/1.380460

Liu, L.G., Chen, C.C., Lin, C.C. and Yang, Y.J., 2005. Elasticity of single-crystal aragonite by Brillouin spectroscopy. *Physics and Chemistry of Minerals*, *32*(2), pp.97-102. doi.org/10.1007/s00269-005-0454-y

Lloyd, S., 1982. Least squares quantisation in PCM. *IEEE transactions on information theory*, *28*(2), pp.129-137. doi.org/10.1109/tit.1982.1056489

Mordy, C.W., Cokelet, E.D., De Robertis, A., Jenkins, R., Kuhn, C.E., Lawrence-Slavas, N., Berchok, C.L., Crance, J.L., Sterling, J.T., Cross, J.N. and Stabeno, P.J., 2017. Advances in ecosystem research: Saildrone surveys of oceanography, fish, and marine mammals in the Bering Sea. *Oceanography*, *30*(2), pp.113-115. doi.org/10.5670/oceanog.2017.230

Moriarty, M., Sell, A.F., Trenkel, V.M., Lynam, C.P., Burns, F., Clarke, E.D., Greenstreet, S.P.R. and McGonigle, C., 2018. Resolution of biodiversity and assemblage structure in demersal fisheries surveys: the role of tow duration. ICES Journal of Marine Science, 75(5), pp.1672-1681. doi.org/10.1093/icesjms/fsy050

Ohman, M.D., Davis, R.E., Sherman, J.T., Grindley, K.R., Whitmore, B.M., Nickels, C.F., and Ellen, J.S., 2019. Zooglider: an autonomous vehicle for optical and acoustic sensing of zooplankton. *Limnology and Oceanography: Methods*, *17*(1), 69-86. doi.org/10.1002/lom3.10301

Olsen, E., Aanes, S., Mehl, S., Holst, J. C., Aglen, A., & Gjøsæter, H. 2010. Cod, haddock, saithe, herring, and capelin in the Barents Sea and adjacent waters: a review of the biological value of the area. *ICES Journal of Marine Science*, 67(1), 87-101. doi.org/10.1093/icesjms/fsp229

Pearcy, W.G., Greenlaw, C.F. and Pommeranz, T., 1983. Assessment of euphausiids with five nets and a 120-kHz echosounder in fjords of northern Norway. *Biological Oceanography*, *2*(2-4), pp.151-177. doi.org/10.1080/00364827.1968.10411128

Pedersen, G., Falk-Petersen, S., Dunlop, K., Camus, L., Daase, M., Basedow, S.L., Bandara, K., Tverberg, V., Pederick, J. and Peddie, D., 2019, June. Autonomous surface vehicles for persistent acoustic monitoring of zooplankton in a highly productive shelf area. In *OCEANS 2019-Marseille.* pp. 1-7. IEEE. doi.org/10.1109/oceanse.2019.8867089

Peña, M., 2019. Mesopelagic fish avoidance from the vessel dynamic positioning system. *ICES Journal of Marine Science*, *76*(3), pp.734-742. doi.org/10.1093/icesjms/fsy157

Proud, R., Cox, M.J., Wotherspoon, S. and Brierley, A.S., 2015. A method for identifying sound scattering layers and extracting key characteristics. *Methods in Ecology and Evolution*, *6*(10), pp.1190-1198. doi.org/10.1111/2041-210x.12396

Proud, R., Cox, M.J., Le Guen, C. and Brierley, A.S., 2018. Fine-scale depth structure of pelagic communities throughout the global ocean based on acoustic sound scattering layers. *Marine Ecology Progress Series*, *598,* pp.35-48. doi.org/10.3354/meps12612

Reiss, C.S., Cossio, A.M., Walsh, J., Cutter, G.R. and Watters, G.M., 2021. Glider-Based estimates of meso-zooplankton biomass density: a fisheries case study on antarctic krill (Euphausia superba) around the northern antarctic peninsula. *Frontiers in Marine Science*, *8*, p.256. doi.org/10.3389/fmars.2021.604043

Rogers, A. D., 2015. Environmental change in the Deep Ocean. *Annual Review of Environment and Resources*. *40*(1), pp. 1–38. doi.org/10.1146/annurev-environ-102014-021415

Santana Hernández, N., 2019. *A patch of Calanus finmarchicus in the Lofoten-Vesterålen Region. Characteristics and determining factors* (Master's thesis, UiT Norges arktiske universitet).

Simmonds, J. and MacLennan, D.N., 2008. *Fisheries acoustics: theory and practice*. John Wiley & Sons. doi.org/10.1002/9780470995303

Skjoldal, H.R., Wiebe, P.H., Postel, L., Knutsen, T., Kaartvedt, S. and Sameoto, D.D., 2013. Intercomparison of zooplankton (net) sampling systems: Results from the ICES/GLOBEC sea-going workshop. *Progress in oceanography*, *108*, pp.1-42. doi.org/10.1016/j.pocean.2012.10.006

Solvang, H.K., Haug, T., Knutsen, T., Gjøsæter, H., Bogstad, B., Hartvedt, S., Øien, N. and Lindstrøm, U., 2021. Distribution of rorquals and Atlantic cod in relation to their prey in the Norwegian high Arctic. *Polar Biology*, *44*(4), pp.761-782. doi.org/10.1007/s00300-021-02835-2

Stanton, T.K., Chu, D., Wiebe, P.H., Eastwood, R.L. and Warren, J.D., 2000. Acoustic scattering by benthic and planktonic shelled animals. *The Journal of the Acoustical Society of America*, *108*(2), pp.535-550. doi.org/10.1121/1.429584

Trevorrow, M.V., Mackas, D.L. and Benfield, M.C., 2005. Comparison of multifrequency acoustic and in situ measurements of zooplankton abundances in Knight Inlet, British Columbia. *The Journal of the Acoustical Society of America*, *117*(6), pp.3574-3588. doi.org/10.1121/1.1920087

Trudnowska, E., Gluchowska, M., Beszczynska-Möller, A., Blachowiak-Samolyk, K. and Kwasniewski, S., 2016. Plankton patchiness in the Polar Front region of the West Spitsbergen Shelf. *Marine Ecology Progress Series*, *560*, pp.1-18. doi.org/10.3354/meps11925

Verfuss, U.K., Aniceto, A.S., Harris, D.V., Gillespie, D., Fielding, S., Jiménez, G., Johnston, P., Sinclair, R.R., Sivertsen, A., Solbø, S.A. and Storvold, R., 2019. A review of unmanned vehicles for the detection and monitoring of marine fauna. *Marine pollution bulletin*, *140*, pp.17-29. doi.org/10.1016/j.marpolbul.2019.01.009

Wiebe, P.H., Boyd, S.H., Davis, B.M. and Cox, J.L., 1982. Avoidance of towed nets by the euphausiid Nematoscelis megalops [Fish behavior]. *Fishery bulletin-United States, National Marine Fisheries Service (USA)*.

Warren, J.D., Stanton, T.K., Wiebe, P.H. and Seim, H.E., 2003. Inference of biological and physical parameters in an internal wave using multiple-frequency, acoustic-scattering data. *ICES Journal of Marine Science*, *60*(5), pp.1033-1046. doi.org/10.1016/s1054-3139(03)00121-8

Whitmore, B.M., Nickels, C.F. and Ohman, M.D., 2019. A comparison between Zooglider and shipboard net and acoustic mesozooplankton sensing systems. *Journal of Plankton Research*, *41*(4), pp.521-533. doi.org/10.1093/plankt/fbz033

Figure captions

Figure 1: Map of the Norwegian Sea and Norway's coasts. The red box in the inset indicates the area shown in the large bathymetric map of Tromsøflaket. The Tromsøflaket map indicates the vessel-based research cruise track in red as it travelled between sampling stations (black stars). Time and GPS location of stations are described in Table 1, and Sailbuoy track in purple is the autonomous acoustic survey. Map produced with cartopy (ver. 0.18.0; scitools.org.uk/cartopy) in orthographic projection and the inset in plate carrée projection (UTM coordinate system).

Figure 2: Example of a) raw pulse-compressed volume backscattering strength (S_v) echogram data upper and lower boundaries of Cluster 0 in red; b) echogram after the mean filtering in time and depth (70 s and 0.09 m filter, respectively); c) projection of raw data by removing the time dimension; and d) projection of filtered data in the depth/S_v dimensions classified into clusters (k=3 in this example) obtained by k-means clustering. In this example, the cluster corresponding to the SSL is Cluster 0.

Figure 3: a-e) Density estimates in the logarithmic domain for each dominant taxonomic group in Tromsøflaket, in units of base 10 logarithm of individuals per m^3. Each box summarises the density measurement from Net (MultiNet; n=11, blue), Trawl (Tucker trawl; n=11, orange), Forward (acoustic forward method; n=70, green) or Inverse (acoustic inverse method; n=70, red). Significant differences are denoted by the number of asterisks (*), with *** $p < 0.001$, ** $p < 0.01$ and * $p < 0.05$ from pairwise Dunn's tests. f) is the total density estimate (sum of all species) for all stations (Net and Trawl) and all SSLs (sound scattering layers) (Forward and Inverse). Note the different y-axis scale in subplot f.

Figure 4: Relative density of each taxonomic group as calculated by each sampling method across the whole survey region of Tromsøflaket with standard deviation error bars representing variability between stations (Net and Trawl) or SSLs (Inverse). Taxonomic groups are ordered from smallest (left) to largest (right). Size details of each taxonomic group are described in Table 4.

Figure 5: Median target strength results of ensemble simulations from the scattering models for each dominant taxonomic group in Tromsøflaket, including the 90%

bootstrap confidence intervals of the median as the shaded region. Vertical grey gashed line indicates the nominal frequency (333 kHz).

Figure 6: The sensitivity analysis results for predicted density estimates of each taxonomic group (a-e) for the inversion of acoustic data with scattering model results varying randomly between median, the 5th and 95th percentiles and the volume backscatter spectra varying randomly between median, and interquartile range for each SSL (x-axis). The blue line in each panel is the median of the sensitivity analysis, the shaded region displays the extent of the 5th and 95th percentile. The red lines indicate the standard deviation of the density estimates for all the SSLs. Note the difference in scale of the y-axis.

Table 1: The location and time of sampling stations within the Tromsøflaket region during the SeaPatches research cruise with R/V Helmer Hanssen.

Station	Date	Time (UTC)	Latitude (°N)	Longitude (°E)
S7	21/06/2018	03:53:00	70.836	17.996
S8	22/06/2018	03:48:00	70.345	19.028
S9	22/06/2018	17:15:00	70.636	18.595
S10	23/06/2018	01:01:00	70.831	18.988
S11	23/06/2018	05:50:00	70.833	18.597
S12	23/06/2018	13:40:00	70.606	18.999
S13	23/06/2018	22:45:00	70.268	18.581
S14	24/06/2018	02:14:00	70.091	18.169
S15	24/06/2018	10:57:00	70.525	18.166
S16	25/06/2018	05:35:00	70.500	16.936
S17	25/06/2018	20:26:00	70.493	17.636

Table 2: PC-DWBA model parameter distributions for each taxonomic group. The distribution used are gamma: Γ(shape, rate), log normal: L(meanlog, sigmalog) and normal: N(mean, sigma).

Parameters	Copepods	Euphausiid larvae	Amphipods
Scattering model	DWBA Prolate spheroid	DWBA Uniformly-bent cylinder	DWBA Uniformly-bent cylinder
Length	N(2.62, 0.09)[a]	L(1.5,0.3)[b]	Γ(10.3, 2.3)[c]
Length-to-width ratio	N(2.7, 0.2)[a]	N(10.5, 0.3)[d]	N(3, 0.5)[d]
Density contrast (g)	N(0.996, 0.003)[e, f]	N(1.036, 0.005)[e]	N(1.058, 0.005)[d]
Sound speed contrast (h)	N(1.027, 0.005)[e]	N(1.026, 0.005)[e]	N(1.058, 0.005)[d]
Orientation	N(90, 30)[g]	N(20, 20)[d]	N(0, 30)[d]

[a] Santana Hernández (2019)

[b] Fit for the length measurements from the Tucker trawl subsamples. The distribution was assessed as the best fit based on a 1:1 line between theoretical and empirical quantile in Q-Q plots.

[c] Fit for the length measurements from MultiNet and Tucker trawl subsamples. The distribution was assessed as the best fit based on a 1:1 line between theoretical and empirical quantile in Q-Q plots.

[d] Lavery et al. (2007)

[e] Kögeler et al. (1987)

[f] Chu and Wiebe (2005)

[g] Blanluet et al. (2019)

Table 3: Viscous elastic model ensemble shape and material properties parameters for pteropods and fish larvae in Tromsøflaket.

Shape (mm)	**Pteropods** *(two-layer sphere)*	**Fish larvae** *(three-layer sphere)*
Radius of elastic shell - R_3	Γ(shape= 5.4, rate= 9.17)[a]	Lognormal(-1.46,0.45)[b]
Radius of viscous layer - R_2	R_3	$(8.77*R_3)+1.62$[c]
Radius of gas layer – R_4	$R_3-(0.023*R_3)$[d]	$R_3-0.01$[e]
Density (kg/m³)		
Surrounding medium – ρ_1	1027[d]	1027[d]
Viscous layer – ρ_2	n/a	1040[e]
Elastic layer – ρ_3	2920[f]	1141[g]
Gas layer – ρ_4	1050[h]	325.1[e]
Sound speed (m/s)		
Surrounding medium – c_1	1480[i]	1480[i]
Viscous layer – c_2	n/a	1522.92[e]
Elastic layer – c_3	5219[e,j]	1450[e]
Gas layer – c_4	1522.92[h,j]	325.1[e]
Shear viscosity (N/m²) - μ_2	n/a	0.8571[e,g]
Shear modulus (MPa) of swimbladder wall - μ_3	35800[j]	0.17[e]

[a] Fit for the length measurements and corresponding widths using length-to-width ratio from Stanton et al. (2000) (L/a = 1.5). The distribution was assessed as the best fit based on a 1:1 line between theoretical and empirical quantile in Q-Q plots.

[b] Swimbladder radius was calculated based on the measured total length and the calculated widths using the relationship described by the data in Chu et al. (2003) and assuming a linear relationship (R^2 = 0.98), as shown in Figure S1. The distribution was assessed as the best fit based on a 1:1 line between theoretical and empirical quantile in Q-Q plots.

[c] Linear regression (Supplementary material; Figure S1) established from swimbladder length-to-total length relationship using data from Chu et al. (2003).

[d] Subtracted shell layer thickness (2.3% of radius) from elastic shell radius based on value from Lavery et al. (2007)

[e] Khodabandeloo et al. (2021)

[f] Stanton et al. (2000)

[g] Feuillade and Nero (1998)

[h] Lavery et al. (2007)

[i] Ship-based CTD measurements

[j] Liu et al. (2005)

Table 4: The size distribution of the dominant species from each taxonomic group. MultiNet and Tucker trawl length measurements were taken from subsamples. The "acoustics" sampling method shows the mean length and standard deviation used in the scattering models for the forward and inverse methods.

Taxonomic group	Sampling method	Species	N	Mean length (mm)	Sd of length (mm)
Pteropods	MultiNet	*Limacina retroversa*	157	1.5	0.6
	Tucker trawl	*Limacina retroversa*	70	1.2	0.3
	Acoustics	*Limacina retroversa*	229	1.4	0.6
Copepods	MultiNet	*Calanus finmarchicus CV*	[a]	2.62[b]	0.09
	Tucker trawl	*Calanus finmarchicus CV*	n/a	n/a	n/a
	Acoustics	*Calanus finmarchicus CV*	[a]	2.62[b]	0.09
Euphausiid larvae	MultiNet	Euphausiacea furcilia	105	4.0	1.0
	Tucker trawl	*Thyssanoessa inermis*	108	4.7	1.6
	acoustics	*Thyssanoessa inermis*	108	4.7	1.6
Amphipods	MultiNet	*Themisto abyssorum*	75	4.6	1.4
	Tucker trawl	*Themisto abyssorum*	108	4.3	1.2
	Acoustics	*Themisto abyssorum*	183	4.4	1.3
Fish larvae	MultiNet	*Pisces larvae*	8	8.3	5.8
	Tucker trawl	juvenile/larvae *Gadus morhua*	61	9.3	3.2
	Acoustics	juvenile/larvae *Gadus morhua*	61	7.6	3.1

Note: All measurements are of full length unless otherwise specified.

[a] Santana Hernández *(2019)*

[b] *Prosome Length (PL)*

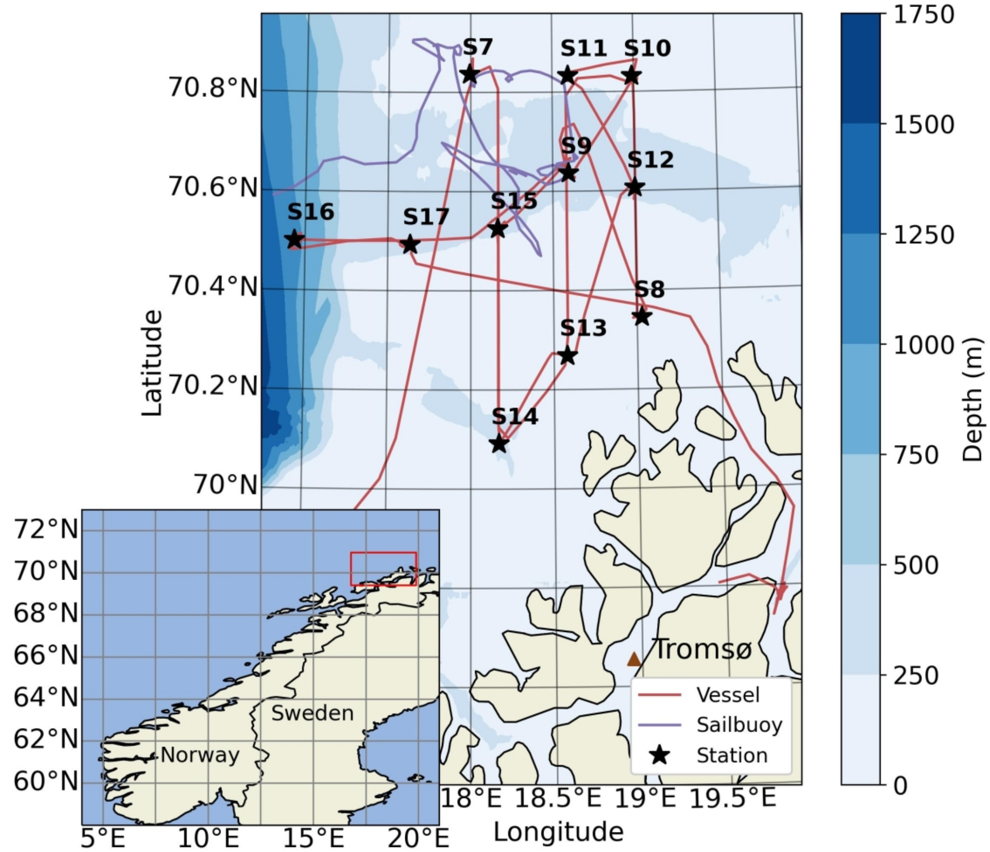

Figure 1: Map of the Norwegian Sea and Norway's coasts. The red box in the inset indicates the area shown in the large bathymetric map of Tromsøflaket. The Tromsøflaket map indicates the vessel-based research cruise track in red as it travelled between sampling stations (black stars). Time and GPS location of stations are described in Table 1, and Sailbuoy track in purple is the autonomous acoustic survey. Map produced with cartopy (ver. 0.18.0; scitools.org.uk/cartopy) in orthographic projection and the inset in plate carrée projection (UTM coordinate system).

198x173mm (300 x 300 DPI)

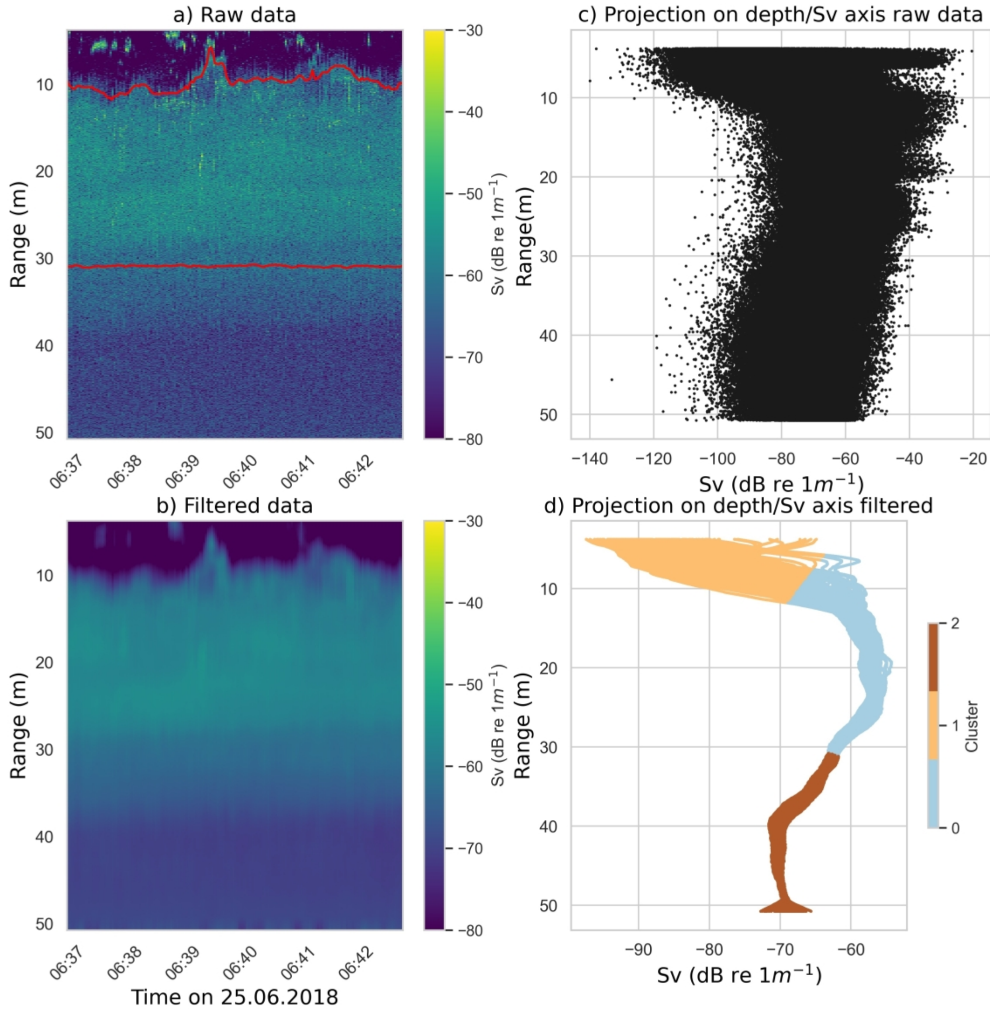

Figure 2: Example of a) raw pulse-compressed volume backscattering strength (Sv) echogram data upper and lower boundaries of Cluster 0 in red; b) echogram after the mean filtering in time and depth (70 s and 0.09 m filter, respectively); c) projection of raw data by removing the time dimension; and d) projection of filtered data in the depth/Sv dimensions classified into clusters (k=3 in this example) obtained by k-means clustering. In this example, the cluster corresponding to the SSL is Cluster 0.

255x261mm (300 x 300 DPI)

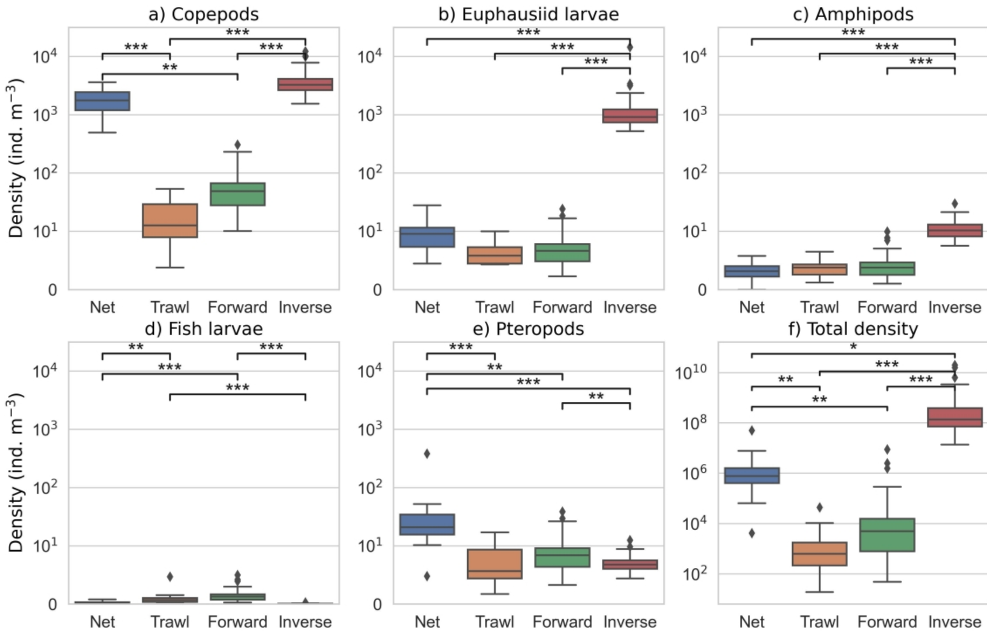

Figure 3: a-e) Density estimates in the logarithmic domain for each dominant taxonomic group in Tromsøflaket, in units of base 10 logarithm of individuals per m^3. Each box summarises the density measurement from Net (MultiNet; n=11, blue), Trawl (Tucker trawl; n=11, orange), Forward (acoustic forward method; n=70, green) or Inverse (acoustic inverse method; n=70, red). Significant differences are denoted by the number of asterisks (*), with *** $p < 0.001$, ** $p < 0.01$ and * $p < 0.05$ from pairwise Dunn's tests. f) is the total density estimate (sum of all species) for all stations (Net and Trawl) and all SSLs (sound scattering layers) (Forward and Inverse). Note the different y-axis scale in subplot f.

299x191mm (300 x 300 DPI)

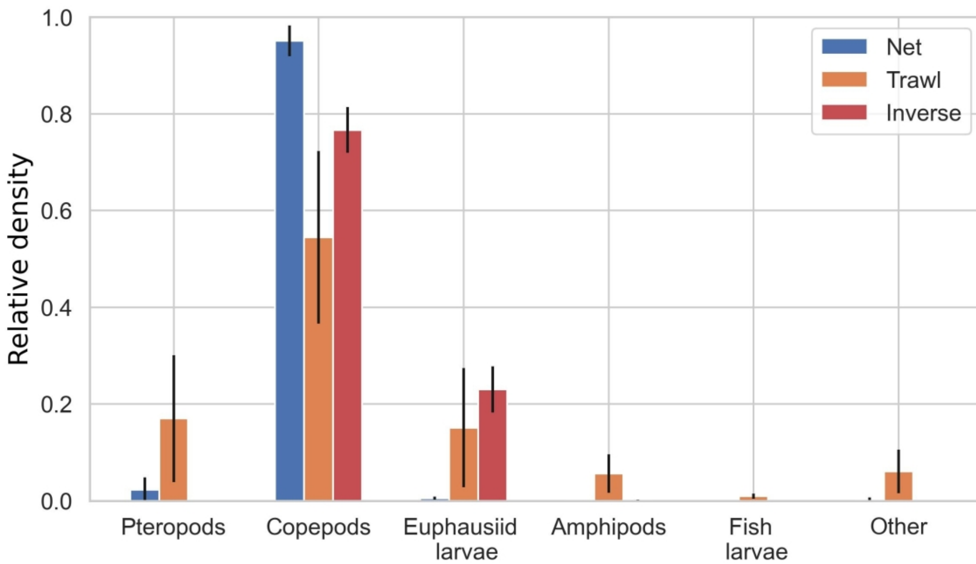

Figure 4: Relative density of each taxonomic group as calculated by each sampling method across the whole survey region of Tromsøflaket with standard deviation error bars representing variability between stations (Net and Trawl) or SSLs (Inverse). Taxonomic groups are ordered from smallest (left) to largest (right). Size details of each taxonomic group are described in Table 4.

198x115mm (300 x 300 DPI)

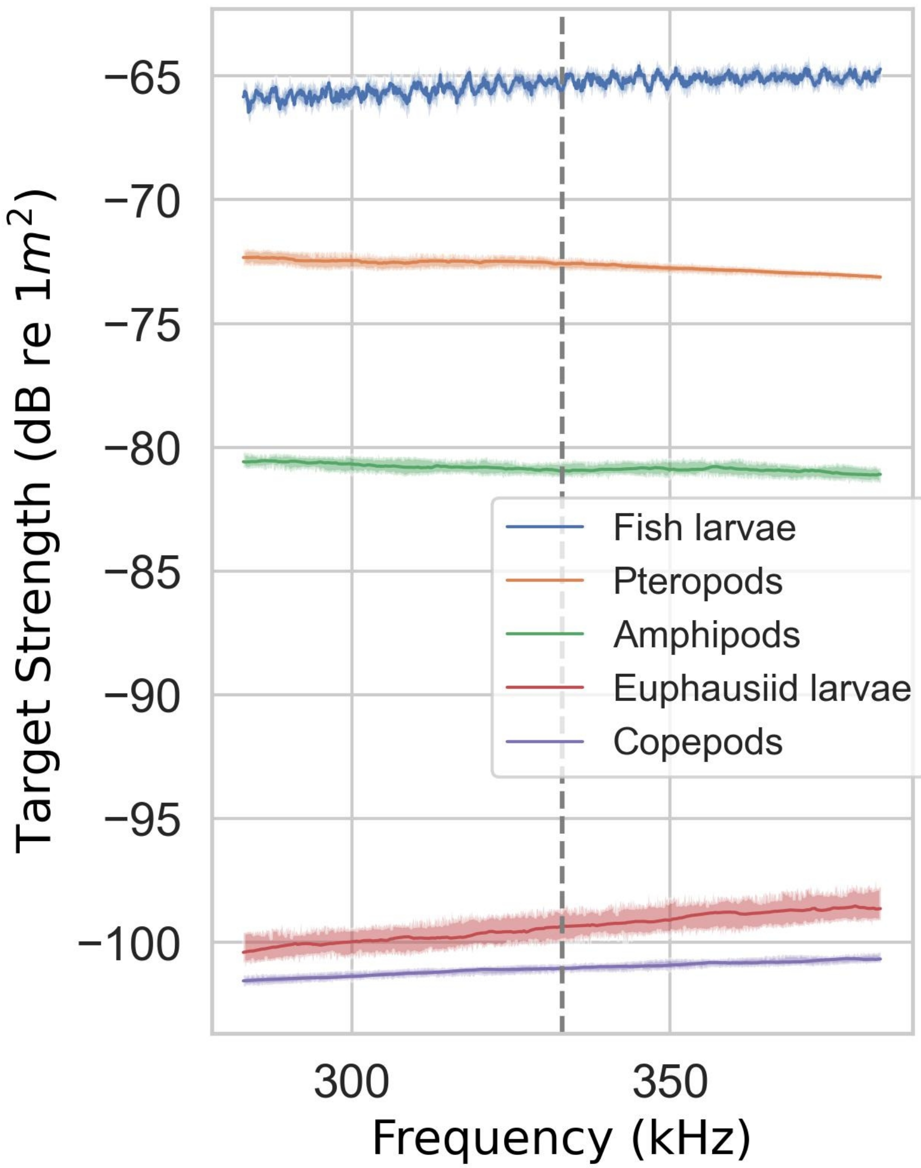

Figure 5: Median target strength results of ensemble simulations from the scattering models for each dominant taxonomic group in Tromsøflaket, including the 90% bootstrap confidence intervals of the median as the shaded region. Vertical grey gashed line indicates the nominal frequency (333 kHz).

108x134mm (300 x 300 DPI)

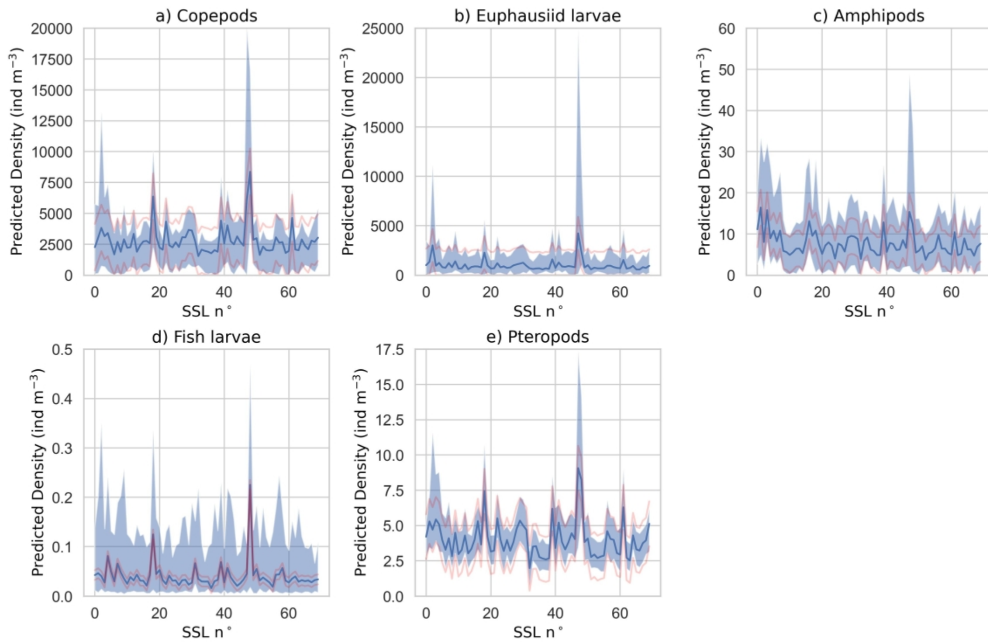

Figure 6: The sensitivity analysis results for predicted density estimates of each taxonomic group (a-e) for the inversion of acoustic data with scattering model results varying randomly between median, the 5th and 95th percentiles and the volume backscatter spectra varying randomly between median, and interquartile range for each SSL (x-axis). The blue line in each panel is the median of the sensitivity analysis, the shaded region displays the extent of the 5th and 95th percentile. The red lines indicate the standard deviation of the density estimates for all the SSLs. Note the difference in scale of the y-axis.

303x196mm (300 x 300 DPI)